Disulfide Bonding Arrangements in Active Forms of the Somatomedin B Domain of Human Vitronectin†

Yuichi Kamikubo,‡ Roberto De Guzman,§ Gerard Kroon,§ Scott Curriden,‡ Jaap G. Neels,‡ Michael J. Churchill,‡ Philip Dawson,‡ Stanisław Ołdziej,# Anna Jagielska,# Harold A. Scheraga,# David J. Loskutoff,*,‡ and H. Jane Dyson*,§

Department of Cell Biology, Division of Vascular Biology, and Department of Molecular Biology and Skaggs Institute for Chemical Biology, The Scripps Research Institute, 10550 North Torrey Pines Road, La Jolla, California 92037, and Baker Laboratory of Chemistry and Chemical Biology, Cornell University, Ithaca, New York 14853-1301

Received February 17, 2004; Revised Manuscript Received April 2, 2004

ABSTRACT: The N-terminal cysteine-rich somatomedin B (SMB) domain (residues 1−44) of the human glycoprotein vitronectin contains the high-affinity binding sites for plasminogen activator inhibitor-1 (PAI-1) and the urokinase receptor (uPAR). We previously showed that the eight cysteine residues of recombinant SMB (rSMB) are organized into four disulfide bonds in a linear uncrossed pattern (Cys^5−Cys^9, Cys^{19}−Cys^{21}, Cys^{25}−Cys^{31}, and Cys^{32}−Cys^{39}). In the present study, we use an alternative method to show that this disulfide bond arrangement remains a major preferred one in solution, and we determine the solution structure of the domain using NMR analysis. The solution structure shows that the four disulfide bonds are tightly packed in the center of the domain, replacing the traditional hydrophobic core expected for a globular protein. The few noncysteine hydrophobic side chains form a cluster on the outside of the domain, providing a distinctive binding surface for the physiological partners PAI-1 and uPAR. The hydrophobic surface consists mainly of side chains from the loop formed by the Cys^{25}−Cys^{31} disulfide bond, and is surrounded by conserved acidic and basic side chains, which are likely to contribute to the specificity of the intermolecular interactions of this domain. Interestingly, the overall fold of the molecule is compatible with several arrangements of the disulfide bonds. A number of different disulfide bond arrangements were able to satisfy the NMR restraints, and an extensive series of conformational energy calculations performed in explicit solvent confirmed that several disulfide bond arrangements have comparable stabilization energies. An experimental demonstration of the presence of alternative disulfide conformations in active rSMB is provided by the behavior of a mutant in which Asn^{14} is replaced by Met. This mutant has the same PAI-1 binding activity as rVN1−51, but its fragmentation pattern following cyanogen bromide treatment is incompatible with the linear uncrossed disulfide arrangement. These results suggest that active forms of the SMB domain may have a number of allowed disulfide bond arrangements as long as the Cys^{25}−Cys^{31} disulfide bond is preserved.

Vitronectin (VN)[1] is a 75-kDa adhesive glycoprotein that is present in blood and in the extracellular matrix of many tissues. It plays a significant role in a number of physiological processes such as cell adhesion, cell migration, modulation of the immune system, and regulation of the plasminogen activation system (*1*, *2*). These functions are mediated through the interaction of VN with a wide variety of structurally dissimilar ligands. For example, VN is anchored to the extracellular matrix via collagen or proteoglycan binding. It promotes cell attachment, spreading, and migration through the interaction of its single Arg−Gly−Asp (RGD) sequence with cellular receptor integrins such as $\alpha_V\beta_3$ (*3*, *4*) and $\alpha_V\beta_5$ (*5*). Unlike other matrix proteins, VN also promotes cell adhesion by binding to urokinase-type plasminogen activator receptor (uPAR) on the cell surface (*6*−*9*). In addition to its adhesive properties, VN also acts as an inhibitor of the cytolytic reactions that occur in the terminal complexes of complement by binding to complement factor C5b-7 (*1*, *2*). VN also binds to type 1 plasminogen activator inhibitor (PAI-1), the primary serine protease inhibitor of both tissue- and urokinase-type plasminogen activators (*10*−*13*). This binding causes a conformational change in the reactive center loop of PAI-1 (*14*) and is thought to stabilize the biological activity of PAI-1 by restricting movement of the central β-sheet A of the inhibitor and preventing insertion of the loop (*15*). Finally, it has been demonstrated that all active PAI-1 in plasma circulates in complex with VN (*10*, *11*, *16*), and that the binding of PAI-1 to fibrin is mediated

† This work was supported by Grants CA27489 (H.J.D.), HL31950 (D.J.L.), and GM14312 (H.A.S.) from the National Institutes of Health and a grant from the Alfred P. Sloan Foundation (P.E.D). R.N.D. is a Special Fellow of the Leukemia & Lymphoma Society.

* Correspondence should be addressed to H.J.D.: phone: 858-784-2223; fax: 858-784-9822; e-mail: dyson@scripps.edu or D.J.L: 858-784-7125; fax: 858-784-7353; e-mail: loskutof@scripps.edu.

‡ Department of Cell Biology, Division of Vascular Biology, The Scripps Research Institute.

§ Department of Molecular Biology and Skaggs Institute for Chemical Biology, The Scripps Research Institute.

Cornell University.

[1] Abbreviations: VN: vitronectin, PAI-1: plasminogen activator inhibitor-1, SMB: somatomedin B; uPAR, urokinase receptor.

10.1021/bi049647c CCC: $27.50
Published on Web 05/08/2004

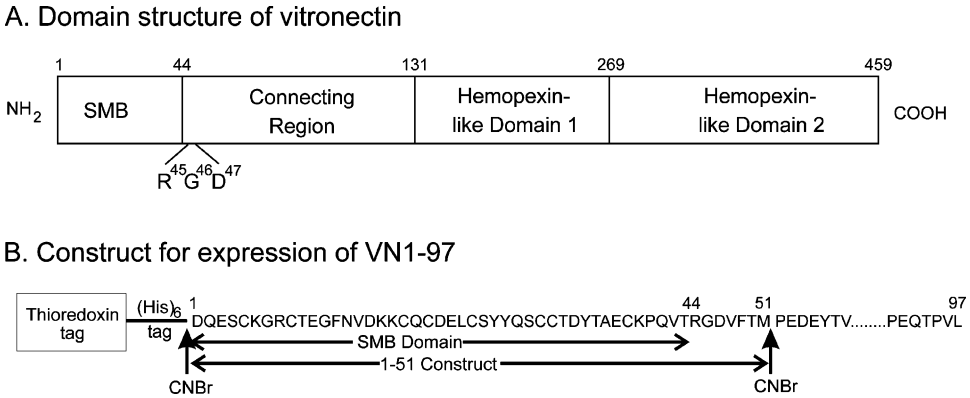

FIGURE 1: (A) Schematic diagram showing the domain structure of vitronectin. (B) Construct used to express the SMB domain. The fragment produced by cyanogen bromide cleavage of VN1−97 contains the RGD adhesion sequence and a homoserine lactone instead of the final methionine residue at position 51. Residues 41−51 of this construct are disordered in solution, according to the NMR spectrum.

by VN (*17*). These results suggest that VN may be a cofactor for PAI-1.

The interaction between VN and PAI-1 may be clinically important since the plasminogen activation system plays a role in physiological processes such as clot dissolution (fibrinolysis) and cell migration, and in pathological processes such as tumor growth and metastasis (*18*, *19*). In fact, elevated levels of active PAI-1 are not only associated with several thrombotic diseases such as myocardial infarction and deep vein thrombosis, but also indicate a poor prognosis for survival in several metastatic human cancers (*20*). These observations may be related to recent studies demonstrating that PAI-1 alters the adhesive properties of cells. For example, it can directly block integrin and uPAR-mediated cell attachment to VN (*8*, *21*), it regulates the migration of cells on VN (*22*, *23*), and it is a potent deadhesive molecule, detaching cells from VN and a variety of other extracellular matrix proteins (*24*).

The mature human VN molecule contains 459 amino acid residues and is organized into four domains that provide the necessarily broad repertoire of binding epitopes needed for target ligands (Figure 1A) (*1*, *2*, *25*). The domain at the N-terminus (amino acids 1−44) is the cysteine-rich somatomedin B (SMB) domain. Interestingly, this domain has also been isolated from human plasma (*26*) and hemofiltrate (*27*) as a separate soluble protein. The single RGD sequence in VN (residues 45−47) is located immediately C-terminal to the SMB domain and is followed by the so-called connecting region (residues 54−130), which contains a putative collagen binding site (*28*). Finally, the two most C-terminal domains in VN have three and four tandem repeat sequences, respectively, with weak homology to sequences in hemopexin. The second hemopexin-like domain (residues 269−459) contains a positively charged heparin-binding region (residues 348−361) (*29*).

The high-affinity binding sites for PAI-1 and uPAR in VN have been localized to the SMB domain (*30*−*33*). Because the affinity of PAI-1 for the SMB domain is much higher than that of uPAR [K_d; 0.27 vs 495 nM, *32*], PAI-1 can competitively inhibit both the binding of uPAR to VN and uPAR-dependent cell adhesion to VN (*8*). Binding of PAI-1 to SMB also inhibits integrin-mediated cell adhesion and migration (*22*, *23*), presumably by sterically blocking the adjacent RGD site (*32*). Interestingly, mature VN is not active in PAI-1 binding, but requires some rearrangement before binding activity is observed. This rearrangement can be achieved in vitro by the addition of a small amount of urea to the protein solution (*32*).

FIGURE 2: Five possible disulfide bond arrangements of the SMB domain of vitronectin. The designations 509, 521, 532, and 539 are for identification purposes, and refer to the disulfide connectivity of residue 5. The 509 arrangement is the one suggested by chemical studies (*34*); the 521 and 539 arrangements were suggested by NMR structure calculations without added disulfide bond restraints (see text). The 532 arrangement is another alternative that preserves both the Cys^{19}−Cys^{21} and Cys^{25}−Cys^{31} disulfide bonds. The 509′ arrangement has the Cys^5−Cys^9 disulfide as in the 509 arrangement, but has the final two disulfides changed to Cys^{25}−Cys^{32} and Cys^{31}−Cys^{39}. The 509′ arrangement is the only one in this series where the Cys^{25}−Cys^{31} disulfide bond is not intact.

The SMB domain of VN contains eight Cys residues, arranged into four disulfide bonds; correct disulfide linkages in this domain are required for PAI-1 binding (*34*−*36*). Neither the disulfide bond arrangement nor the structure of the SMB domain within native VN has been determined, probably due to the technical difficulty of preparing the native SMB domain. We recently isolated the recombinant form of active SMB (rSMB) from transformed *Escherichia coli* and presented data to suggest that the four disulfide bonds were arranged consecutively in a linear uncrossed pattern (Cys^5−Cys^9, Cys^{19}−Cys^{21}, Cys^{25}−Cys^{31}, and Cys^{32}−Cys^{39}) (*34*). We have designated this as the disulfide bond arrangement 509 (Figure 2; the nomenclature used to designate the disulfide bond arrangement indicates the pairing of Cys^5). More recently, Zhou et al. (*37*) reported the X-ray crystal structure of the SMB domain in complex with the physiological partner PAI-1. The SMB domain structure in this complex showed a crossed disulfide pattern, the same as one that we term 521 (Figure 2) (Cys^5−Cys^{21}, Cys^9−

Cys^{39}, $Cys^{19}-Cys^{32}$, and $Cys^{25}-Cys^{31}$). Surprisingly, no mention was made in this report (*37*) of the previously published evidence for a different disulfide bond arrangement (*34*).

In this article, we report three new experimental findings related to this question. First, the solution structure of the SMB domain has been determined by NMR analysis, using both unlabeled and ^{15}N-labeled recombinant SMB (rSMB). A number of different disulfide arrangements were able to satisfy the NMR restraints, with comparable stabilization energies according to an extensive series of conformational energy calculations. Regardless of the variations in the internal disulfide pattern, the critical residues in the PAI-1 binding site, previously mapped by mutagenesis (*35*, *38*), form a cluster on the surface along the loop formed by the $Cys^{25}-Cys^{31}$ disulfide bond, and appear to be poised for interaction with physiological partners. Second, further evidence is presented for the presence of the linear disulfide arrangement 509, obtained using a different method. Finally, evidence is presented that an alternative disulfide arrangement, not including the Cys^5-Cys^9 disulfide, is compatible with nativelike biological activity. These results suggest that the active SMB domain may be permitted considerable disulfide bond heterogeneity or variability, provided that the $Cys^{25}-Cys^{31}$ disulfide bond is preserved.

MATERIALS AND METHODS

Materials. All chemicals were the highest analytical grade commercially available. Materials were obtained as follows: cyanogen bromide (CNBr), ampicillin, kanamycin, and carbenicillin were from Sigma (St. Louis, MO); trifluoroacetic acid was from Pierce (Rockford, IL); HPLC-grade acetonitrile was from EM Science (Gibbstown, NJ); isotopically labeled compounds $^{15}NH_4Cl$ and $(^{15}NH_4)_2SO_4$ were from Isotec (Miamisburg, OH). Urea-activated VN was purified as described by Yatohgo et al. (*39*). Anti-VN monoclonal antibody (mAb) 153 was generated in mice immunized with urea-activated human VN as reported (*31*). The recombinant stable active form of human PAI-1 was purified from transformed *E. coli* BL21 cells (clone 14-1b; a kind gift from Dr. Daniel A. Lawrence) according to the method described previously (*40*).

A synthetic SMB peptide, $Asp^{22}Glu^{23}Leu^{24}Cys^{25}Ser^{26}Tyr^{27}Tyr^{28}Gln^{29}Ser^{30}Cys^{31}$ (VN22−31), which contains the $Cys^{25}-Cys^{31}$ disulfide bond, was synthesized on an Applied Biosystems 433a peptide synthesizer using in situ neutralization/HBTU activation protocols for Boc chemistry (*41*). The peptide was purified by RP-HPLC on a Waters Deltaprep 4000 using a Vydac C18 column and acetonitrile/water/0.1% TFA gradients. Boc-amino acids and HBTU were purchased from Peptides International (Louisville, KY). *p*-Methylbenzhydramine (MBHA) resin was purchased from Peninsula (San Carlos, CA). The C-terminal carboxyl group was amidated. The fidelity of the peptide was ascertained by matrix-assisted laser desorption/ionization time-of-flight mass spectrometry (Mass Spectrometry Core facility, the Scripps Research Institute). The properly folded peptide in the mixture was purified as previously described (*34*), using a conformation-specific monoclonal antibody.

Expression of the rSMB Domain of Human VN. In the present study, the SMB domain of human VN was expressed in transformed *E. coli* as a fusion protein containing the NH_2-terminal 97 amino acid residues (VN1−97) linked to the COOH-terminus of thioredoxin and a His_6 tag region as described previously (*34*) (see Figure 1B). In brief, for construction of the expression vector, DNA encoding VN1−97 was amplified from human VN cDNA (*42*) by PCR using the 5′-oligonucleotide primer, 5′-TAGAACGTCCATGGACCAAGAGTCATGCAAG-3′, and the 3′-oligonucleotide primer, 5′-AGTACTCGAGTCACAGAACAGGTGTCTGCTCA-3′, and was then cloned into the pET-32a (+) expression vector (Novagen, Madison, WI) using NcoI and XhoI sites. To prepare cells expressing recombinant VN1−97 (rVN1−97), *E. coli* strain BL21*trxB* (DE3) (Novagen) was transformed with the above plasmid DNA, and grown at 37 °C in 2 × YT medium containing ampicillin (100 μg/mL) and kanamycin (15 μg/mL) to a density of approximately 2×10^8 cells/mL. To induce the expression of rVN1−97, the cells were then transferred to room temperature, and isopropyl-β-D-thiogalactopyranoside was added to the medium to a final concentration of 0.5 mM. After induction for 2.5 h, the cells were collected by centrifugation and suspended in 20 mM Tris-HCl (pH 8.0) containing 0.1 M NaCl. The cell suspension was stored at −70 °C. For ^{15}N-labeling of VN1−97, 10 mL of the cells, which had been previously cultured in LB medium, were transferred to 4 L of M9 minimal medium that was supplemented with 4 g of $^{15}NH_4Cl$, 4 g of $(^{15}NH_4)_2SO_4$, and 40 g of glucose. The cells were further cultured in the presence of carbenicillin (100 μg/mL) at 37 °C, and then the expression of ^{15}N-labeled VN1−97 was induced as described above.

A mutant (rVN1−97$Asn^{14} \rightarrow$ Met), in which Asn^{14} was replaced by Met, was constructed in the VN1−97 background by oligonucleotide-directed site-specific mutagenesis using a QuickChange Site-Directed Mutagenesis kit (Stratagene, La Jolla) and the forward primer 5′-CCGCTGCACTGAGGGCTTCATGGTGGACAAGAAGTGCC-3′ and the reverse primer 5′-GGCACTTCTTGTCCACCATGAAGCCCTCAGTGCAGCGG-3′. For expression of this protein, the construct was ligated into the pET-32a (+) expression vector, and the plasmid was transformed into *E. coli* strain AD494 (DE3) pLysS (Novagen). Recombinant protein was expressed using standard procedures.

Preparation of rVN1−51 Containing the SMB Domain. To prepare a smaller VN peptide containing the SMB domain for NMR analysis, we cleaved rVN1−97 with CNBr, and subsequently performed immunoaffinity chromatography as described previously (*34*) to purify the NH_2-terminal 51 amino acids (VN1−51). Following induction and expression of rVN1−97, the cell suspension was lysed by using a Pressure Cell Press (Spectronic Instruments, Rochester, NY), and the resulting supernatant containing rVN1−97 was then applied to an affinity column containing His-bind resin (Clontech, Palo Alto, CA). For preparation of active recombinant VN1−51 (rVN1−51), 60 mg of rVN1−97 was reacted with 80 mg of CNBr in 70% (v/v) aqueous trifluoroacetic acid for 24 h at room temperature. The reaction product was dried, dissolved in water, and dialyzed against 50 mM Tris-HCl (pH 7.4) containing 0.1 M NaCl at 4 °C. After dialysis, to isolate the active rVN1−51, the cleaved rVN1−97 was applied to an anti-VN mAb 153-conjugated Cellufine column (1.0 × 6 cm) and, after washing with 50 mM Tris-HCl (pH 7.4) containing 1 M NaCl, bound rVN1−

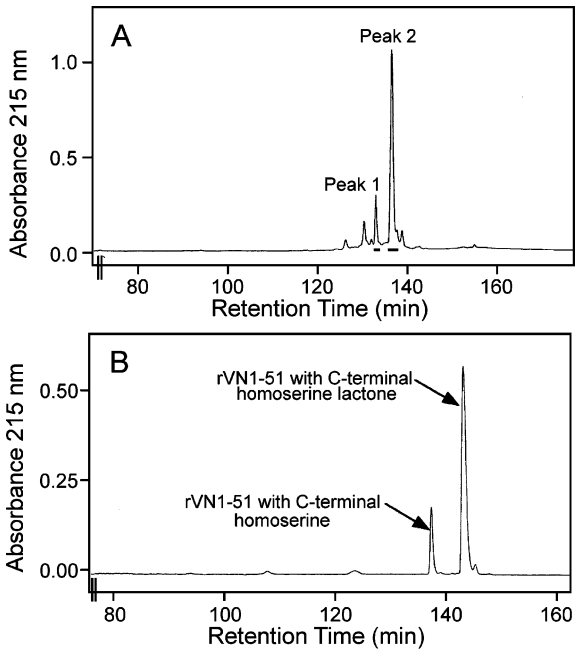

FIGURE 3: (A) Reversed phase chromatograph (BetaBasic CN column in 0.1% (v/v) aqueous trifluoroacetic acid, eluted with a gradient of acetonitrile) showing purification of active rVN1−51. The solid line shows the absorbance of the eluate at 215 nm. Active rVN1−51 containing either a C-terminal homoserine (molecular mass of 5781 Da) or a C-terminal homoserine lactone (molecular mass of 5763 Da) was detected in main peaks 1 and 2, respectively. (B) Analytical reversed phase chromatography (Vydac C18 column with a linear gradient (from 15 to 30%) of 80% acetonitrile in 0.1% (v/v) aqueous trifluoroacetic acid) of purified rVN1−51 containing a C-terminal homoserine lactone. The chromatogram shows that the purified rVN1−51 had high (>90%) purity, although part of the rVN1−51 was converted to the other active form of rVN1−51 with a C-terminal homoserine.

51 was eluted with 0.1% (v/v) aqueous trifluoroacetic acid. The column was regenerated by equilibrating it with 50 mM Tris-HCl (pH 7.4) containing 0.1 M NaCl. We performed the affinity chromatography at 4 °C. For further purification of the active rVN1−51, the eluted rVN1−51 was subjected to reversed phase chromatography using a BetaBasic CN column (21.2 × 150 mm, Western Analytical Products, Murrieta, CA) with a linear gradient (from 0 to 55%) of 80% acetonitrile in 0.1% (v/v) aqueous trifluoroacetic acid at a flow rate of 6 mL/min. The reversed phase chromatography was also performed at 4 °C. In the reversed phase chromatogram, active rVN1−51 containing either a C-terminal homoserine (molecular mass of 5781 Da) or a C-terminal homoserine lactone (molecular mass of 5763 Da) was detected in main peaks 1 and 2, respectively (Figure 3A). Finally, after lyophilization of the purified rVN1−51 containing a C-terminal homoserine lactone, the resulting powder was dissolved in 20 mM sodium phosphate buffer (pH 7.5) and the solution was kept at −80 °C before the NMR analysis and disulfide bond study. To check the purity of the rVN1−51 preparation, we performed an analytical reversed phase chromatography using a Vydac C18 column (4.6 × 250 mm, Western Analytical Products) with a linear gradient (from 15 to 30%) of 80% acetonitrile in 0.1% (v/v) aqueous trifluoroacetic acid at a flow rate of 0.5 mL/min. The chromatogram showed that purified rVN1−51 with a C-terminal homoserine lactone had high (>90%) purity, although part of the rVN1−51 was converted to the other active form of rVN1−51 with a C-terminal homoserine (Figure 3B).

rVN1−51Asn^{14} → Met and ^{15}N-labeled rVN1−51 were prepared in the same way following CNBr cleavage of rVN1−97Asn^{14} → Met and ^{15}N-labeled rVN1−97, respectively. The average masses of all VN variants were determined by matrix-assisted laser desorption/ionization time-of-flight mass spectrometry (Mass Spectrometry Core Facility, The Scripps Research Institute, La Jolla, CA), and their concentrations were determined by amino acid composition analysis (Protein and Nucleic Acids Core Facility, The Scripps Research Institute).

Determination of PAI-1 Binding Activity. The PAI-1 binding activities of rVN1−51, rVN1−51Asn^{14} → Met, and ^{15}N-labeled rVN1−51 were determined by competitive surface plasmon resonance (SPR) analysis using a BIAcore 3000 biosensor system and reagents (amine-coupling kit and CM5-sensor chips) from BIAcore AB (Uppsala, Sweden). To prepare urea-activated VN-immobilized sensor chips, 20 μg/mL of VN in 10 mM acetate buffer (pH 4.0) was injected onto the sensor chips (CM5) and immobilized by using an amine coupling kit as described by the supplier. A control channel was activated and blocked in the absence of protein. Binding to coated channels was corrected for binding to the uncoated channel. SPR analysis was assessed in BIAcore certified HBS-EP buffer (10 mM HEPES, pH 7.4, 0.15 M NaCl, 3 mM EDTA, and 0.005% surfactant P20). The PAI-1 sample (25 nM), which had been preincubated with various concentrations of rVN1−51, rVN1−51Asn^{14} → Met, or ^{15}N-labeled rVN1−51 at room temperature for 10 min, was passed over the sensor chip with a flow rate of 20 μL/min. The amount of bound PAI-1 on the sensor chip was determined by measuring the resulting signal expressed as resonance units. All experiments were performed at 25 °C, and the sensor chip was regenerated by washing with 0.1 M HCl. The PAI-1 binding activity of the various rVN1−51 molecules was also determined by competitive binding assay using a VN-coated microtiter plate as described previously (*34*). The PAI-1 binding activities were the same before and after NMR spectroscopy.

Binding Affinity of SMB Peptide VN22−31 for anti-VN mAb. The binding affinity of rVN1−51, rVN1−51Asn^{14} → Met, and the synthetic SMB peptide VN22−31 was determined by competitive BIAcore experiments using urea-activated VN-immobilized sensor chips as described in the previous section. Varying concentrations of the SMB peptides were incubated with 25 nM mAb 153 at room temperature for 60 min, and then injected onto the chip. A control experiment demonstrated that mAb 153 bound to urea-activated VN on the sensor chip with a K_d value of 3.0 nM (data not shown).

Disulfide Bond Arrangement of rVN1−51. The disulfide arrangement of rVN1−51 was previously determined by partial reduction and alkylation using TCEP to minimize disulfide exchange (*34*). In the present study, the disulfide bond arrangement of this domain was determined by peptide mapping analysis of cleavage products that resulted from partial acid hydrolysis of rVN1−51 according to the method described by Derua et al. (*43*). The analysis was performed utilizing a combination of liquid chromatography/electrospray ionization mass spectrometry (LC/ESI-MS) and peptide recognition software (F-MASS and F-LINK programs: http://

criproteomics.usouthal.edu/peptide/). rVN1−51 was partly acid-hydrolyzed by incubating rVN1−51 powder (1.8 nmol) with 300 μL of 0.5 M HCl at 110 °C for 3 h. After lyophilization of the hydrolysis mixture, the powder was dissolved in 0.1% (v/v) aqueous trifluoroacetic acid, and this solution was applied to LC/ESI-MS using an Agilent 1100 LC system coupled to a Micromass LCT instrument (Mass Spectrometry Core Facility, The Scripps Research Institute). In the LC system, cleavage products were separated by reverse-phase chromatography using a Vydac C8 column (4.6 × 250 mm). To characterize the resultant peptides, the observed masses of each fragment determined by ESI-MS were first analyzed using the F-MASS program to identify all nondisulfide-linked fragments. These fragments were eliminated from the analysis, and the remaining fragments containing disulfide bonds were subsequently analyzed using the F-LINK program. This analysis revealed the total number of times that each theoretical disulfide arrangement was inconsistent with the presence of an observed cleavage product.

NMR Spectroscopy. NMR spectra of unlabeled and ^{15}N-labeled rVN1−51 were recorded on Bruker DRX600, Avance750, or Avance900 spectrometers at 293 K, processed using NMRPipe (*44*), and analyzed using NMRView (*45*). Backbone resonances were assigned from three-dimensional ^{15}N TOCSY−HSQC and ^{15}N NOESY−HSQC spectra at 600 and 750 MHz and from two-dimensional 2QF COSY and NOESY spectra at 900 MHz.

Restraint Generation. Interproton upper bound distance restraints were derived from cross-peak intensities in the 3D ^{15}N NOESY−HSQC and 2D NOESY spectra. Distance restraints were assigned upper bounds of 2.5, 3.0, 4.0, 5.0, and 6.5 Å, and lower limits were set to the van der Waals contact distance (1.8 Å). Backbone φ and ψ torsion angle restraints were obtained using chemical shift data and the pattern of medium-range NOE connectivities (*46*−*49*). Table 1 shows the numbers of restraints used in the structure calculations. The published disulfide arrangement (*34*) was used in initial structure calculations. Subsequent parallel calculations used the published arrangement (509) and two candidate "crossed" disulfide patterns (521 and 539, Figure 2) inferred from the initial structures. Disulfide bond distances were restrained to 2.00−2.10 Å (*50*). All ambiguous restraints in each dataset were assigned upper bounds of 6.5 Å, but were omitted in the initial DYANA and AMBER calculations.

Structure Calculation and Analysis. An initial set of 200 SMB structures was calculated using unambiguous NOE and torsion angle restraints in the program DYANA (*50*). The 100 structures with the lowest target functions were imported into AMBER 7 (*51*) using a parm99 force field (*52*), 20 kcal/mol·Å^2 force constant on interproton distance restraints, and 150 kcal/mol for torsion angle restraints.

Restraints were ramped from 4 to 20 kcal/mol in the first 12-ps (ps, 1 time step = 1 fs) cycle of simulated annealing (1000 K) and were ramped from 4 to 20 kcal/mol during a second 20-ps annealing step (500 K). In an 8-ps third round of annealing at 0 K, restraints were maintained at 20 kcal/mol. Sixty low energy structures were transferred into a full-charge force field (ff99) and subjected to one 20-ps round of simulated annealing at 1000 K using a generalized Born solvent model (*53*−*56*). Twenty structures with the lowest combined distance and angle violations were sorted by AMBER energy and selected for analysis. Backbone analysis was performed using PROCHECK (*57*) and PROMOTIF (*58*). Graphics images were prepared using MOLMOL (*59*) and GRASP (*60*).

Table 1: Experimental Restraints and Structural Statistics

NMR Restraints	
total unambiguous distance restraints	1010
intraresidue	406
sequential	188
medium range	237
long range	179
ambiguous distance restraints	314
total dihedral angle restraints	69
ϕ	45
ψ	24

Ensemble Statistics (20 structures each)

disulfide arrangement:	509	521	539
violation analysis			
maximum distance violation (Å)	0.28	0.32	0.23
maximum dihedral angle violation (°)	26	20	26
energies			
mean restraint energy (kcal mol^{-1})	5.8	4.1	4.8
mean AMBER energy (kcal mol^{-1})	−2052	−2099	−2088
RMS deviation from the average structure (S4-K40)			
backbone atoms (N,C$^\alpha$,C′) (Å)	0.57	0.68	0.71
all heavy atoms (Å)	1.00	1.17	1.19
deviation from idealized geometry			
bond lengths (Å)	0.01	0.01	0.01
bond angles (°)	2.0	2.0	2.0
Ramachandran plot			
most favorable regions (%)	63.3	70.7	70.4
additionally allowed regions (%)	36.2	28.3	28.8
generously allowed regions (%)	0.4	1.0	0.8
disallowed regions (%)	0.0	0.0	0.0

Coordinates. The assigned chemical shift list has been deposited in the BioMagResBank with accession number 6160 and the coordinates in the Protein Data Bank with accession number 1SSU.

Conformational Energy Calculations. An extensive search was carried out in the conformational space of the SMB protein to determine the global fold and to help in the initial NMR structure calculations, as well as to provide an independent assessment of the experimentally determined disulfide bond arrangement or possible different disulfide bond arrangements consistent with the NMR data. A shorter form of the VN1−51 sequence (residues 1−41, termed VN1−41) was used, since the NMR data indicated that the 10-residue C-terminal tail was unstructured. A united-residue (UNRES) force field (*61*), with implicit inclusion of solvent through side chain−side chain interactions, and a conformational-space annealing (CSA) search procedure (*62*), were used in the initial calculations. The UNRES/CSA procedure uses only information about the amino acid sequence of the chain. No restraints were imposed in any of the UNRES runs to force formation of disulfide bonds, and no NMR information was used at this stage to calculate the structures. The conformational ensemble was clustered with a minimal tree algorithm (*63*), and the conformations were then filtered using the minimal amount of initially available NMR data to select those that satisfied the NOE restraints. The initial NMR data used for filtering consisted of 112 unambiguous NOEs, viz., 45 sequential (i,i+1), 46 medium-range (i,i+2

to i,i+4), and 21 long-range (greater than i,i+4). The best conformation of VN1−41, based on the UNRES energy and the ability to accommodate the available NMR restraints was converted to an all-atom representation (*64*). Five disulfide bond arrangements (509, 509′, 521, 532, and 539; Figure 2) were found to be possible in the resulting preliminary structure.

To determine the most likely of these five plausible arrangements in the solution structure, molecular dynamics calculations in explicit water were carried out for each of these five models, using the X-ray coordinates (chain B of the 1OCO PDB structure (*37*), residues 3−39) as the starting geometry. All molecular dynamics calculations, as well as energy minimizations, were carried out with the AMBER 7 program (*51*) and the parm99 all-atom force field (*52*), with TIP3P water (*65*) and the Ewald summation for electrostatic interactions, at 300 K.

To close the disulfide bonds in each of the five arrangements, the energies of the all-atom models were initially minimized in a vacuum with a distance-dependent dielectric constant ($4r_{ij}$, where r_{ij} is the distance between atoms *i* and *j*), and then in a box of TIP3P water molecules. Disulfide bonds were formed with a loop-closing potential. In all five energy-minimized models, the lengths of the disulfide bonds adopted physically reasonable values, about 2 Å between sulfur atoms, without significant changes of the initial (X-ray) structure (the RMSD of the α-carbon atoms between the X-ray and the energy-minimized structures was less than 2 Å).

Two types of molecular dynamics calculations were carried out, viz., with NOE distance restraints and unrestrained. One-nanosecond restrained molecular dynamics calculations were carried out to check which of the five models could satisfy the experimental NMR data. The restraints were introduced into the potential as a penalty in the form of a Gō-type function (*66*), i.e., a well with a flat bottom, parallel linear sides in ranges depending on the deviations defined by 650 experimental distance restraints obtained from the NOEs, and a force constant of 20 kcal/mol·Å^2, were used. Additionally, unrestrained 1-ns molecular dynamics calculations were carried out to analyze the disulfide arrangements, independent of the NMR data, to obtain results unaffected by possible errors in the experimental data.

The molecular dynamics trajectories for all five models in restrained and unrestrained calculations were stable, and were used for further analysis, viz., to calculate average (conformational plus hydration) energies, using the generalized Born (GB) approach (*53*−*55*, *67*) for the electrostatic part of the hydration energy and the solvent accessible surface area (SA) model (*67*) for the nonelectrostatic part. The energies, average torsional angles for the disulfide bonds, C−S−S−C, and the average deviations from the NMR distance restraints were compared for all models.

RESULTS

NMR Spectra of rVN1−*51*. NMR data were initially obtained with an extremely small, low concentration protein sample labeled with ^{15}N (0.35 mL of a 200 μM solution). The ^{15}N−^{1}H HSQC spectrum obtained with this material is shown in Figure 4. The dispersion of the cross-peaks in the spectrum indicates that the protein is folded, and the number of cross-peaks is consistent with a single dominant conformation. The resonance line widths are consistent with a monomeric protein of the correct molecular weight. Additional data were obtained with a more concentrated sample of unlabeled protein, for which standard ^{1}H 2D NMR data were obtained. The NMR spectra indicated that the COOH-terminal 10 residues of the cyanogen bromide fragment 1−51 were disordered in solution. Relatively sharp resonances were observed for these residues, and the chemical shifts for residues 42−51 were indicative of the absence of secondary structure. In addition, only intraresidue and sequential (i,i+1) NOEs were observed for this region of the polypeptide. These observations indicate that the COOH-terminus is unfolded in solution and does not interact with the folded cysteine-rich SMB domain. It has therefore been omitted from the structure diagrams.

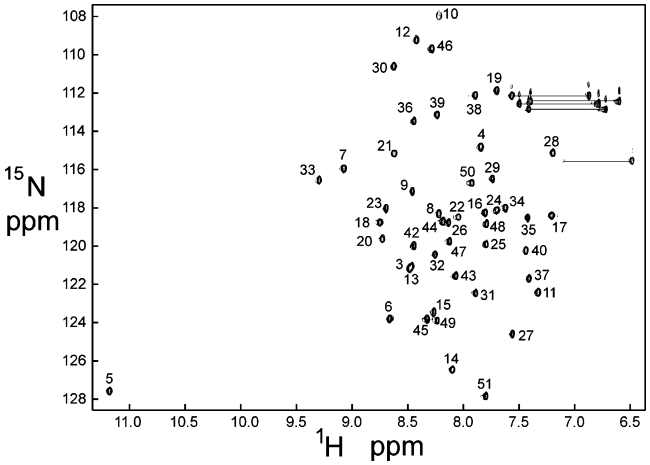

FIGURE 4: ^{1}H−^{15}N HSQC spectrum of fully active ^{15}N-labeled rVN1−51 at 283 K. The protein concentration was approximately 200 μM in 20 mM sodium phosphate buffer, pH 7.5. ^{1}H−^{15}N cross-peaks corresponding to backbone amides are labeled with the residue number. Asparagine and glutamine side chain amides are connected by a horizontal line.

Solution Structure of rVN1−*51*. The SMB domain, despite its small size, presented significant problems for solution structure determination in the absence of good isotopically labeled samples. Such a small domain (<40 residues in the folded portion) would generally be unstructured in solution without the conformational restraint supplied by the disulfides. The presence of multiple disulfide bonds in a small domain obviates the need for the well-packed hydrophobic cores that provide the majority of the stability of most proteins. However, protein NMR structure calculations rely heavily on the high density of long-range distance restraints provided by the hydrophobic interactions in the core of the protein. Small cysteine-rich domains frequently have a relatively low density of NOEs in the center of the molecule, which can pose problems for high-resolution solution structure determination. In the case of the SMB domain, this is exacerbated by the almost total absence of hydrophobic residues other than the disulfide-bonded cysteines. In addition, a number of the resonances of the Cys residues were overlapped. Therefore, we utilized an iterative method to calculate and refine the structures. In initial calculations, only NOEs that could be unambiguously assigned were utilized, together with our previously published disulfide arrangement (*34*), to establish an overall fold. The next step in the iterative

process utilized a set of backbone dihedral angle restraints, derived from inspection of chemical shift index, patterns of sequential and intraresidue NOEs, and a limited data set of coupling constants available from the ^{1}H spectra. In this intermediate calculation, the force field of the backbone dihedral angle restraints was set at a higher value than normal. This method has been used previously to define the global fold of a small domain, and to identify possible conflicting or erroneous NOE restraints (*68*). In subsequent calculations, the force field for dihedral angle restraints was returned to normal values. NOEs identified as possibly erroneous or conflicting were removed from the restraint list, and a further round of structure calculations was made. The structures obtained from this round of calculations were used as a means to identify further NOE restraints from the spectra, utilizing a protocol in the program NMRview (*45*) similar to the SANE calculation (*69*). Successive rounds of NOE assignment and structure calculation gave a final set of structures with acceptable RMSD, violations, and energies. The final round of structure calculations utilized a restrained molecular dynamics calculation with additional refinement with a generalized Born (GB) continuum solvent model (*53*−*56*).

These calculations yielded a well-determined structure family, with low restraint violations and low root-mean-square deviation (RMSD) between members of the family for the backbone of the structured region. Overall energies were acceptable, and the backbone RMSD for the structured portion of the protein was small. The structures showed that the disulfide bonds were clustered in the center of the molecule, in extremely close proximity. All of the sulfur atoms of the Cys residues were within approximately 5 Å of each other, raising the possibility that other disulfide arrangements could also be consistent with the NMR restraints. The disulfide bonds provide the only stabilization for the folded structure of the SMB domain. However, the disulfide bonds in the linear arrangement provide only local restraints: they do not provide long-range restraints that might reasonably be expected to stabilize the domain.

Solution Structures with Alternative Disulfide Arrangements. To investigate the possibility of alternative disulfide arrangements, we performed a structure calculation without disulfide restraints. This calculation indicated that two other, nonsequential, disulfide arrangements were compatible with the NMR spectra, one termed 521 (Cys^5−Cys^{21}, Cys^9−Cys^{39}, Cys^{19}−Cys^{32}, and Cys^{25}−Cys^{31}) and the other termed 539 (Cys^5−Cys^{39}, Cys^9−Cys^{21}, Cys^{19}−Cys^{32}, and Cys^{25}−Cys^{31}) (Figure 2). Interestingly, all of these disulfide arrangements contain the Cys^{25}−Cys^{31} disulfide bond. The three possible sets of structures (i.e., 509, 521, 539) were refined in parallel, with structure calculations utilizing the same complete set of NOEs and a limited set of backbone dihedral angle restraints, mainly in the two regions where a single helical turn was observed. Families of 20 structures for these three disulfide arrangements are shown in Figure 5 and structure statistics for the three final refined structure families are shown in Table 1. Single structures for each of the three arrangements are shown in Figure 6; the backbones superimpose with an RMSD of 0.83. It is clear that the overall fold is identical in all three cases. The energies are quite similar for all three arrangements (Table 1).

Determination of the Disulfide Bond Arrangement of rVN1−*51 by Acid Hydrolysis.* Although we previously showed (*34*) that the disulfide bonds in active rSMB were arranged in a linear uncrossed pattern (509, Figure 2), Zhou et al. (*37*) showed a crossed disulfide pattern (equivalent to 521, Figure 2) for rSMB in a complex with PAI-1. These differences could reflect differences in the samples analyzed (e.g., SMB in solution vs SMB in PAI-1/SMB crystals), or shuffling of the disulfide bonds during the chemical cleavage process or during crystallization, or selection of a particular disulfide bond arrangement from a heterogeneous mixture during crystallization of the SMB−PAI-1 complex. To explore the possibility that the disulfides might have been rearranged during the previous chemical analysis by partial reduction and alkylation (*34*), we undertook to repeat the analysis using a different method. Derua et al. (*43*) previously reported that acid hydrolysis under controlled conditions provides fragmentation of cysteine-rich peptides without disulfide-bond scrambling. Therefore, we reexamined the disulfide-bond arrangement of the SMB domain employing this approach. We performed a peptide mapping analysis of the cleavage products that result from partial acid hydrolysis of rVN1−51, utilizing a combination of reverse phase chromatography and electrospray ionization mass spectrometry (LC/ESI-MS). After LC/ESI-MS, we employed peptide recognition software to determine the disulfide bond arrangement. We first used the F-MASS program to eliminate all nondisulfide-bonded peptide fragments in the acid-cleaved rVN1−51. We subsequently identified all of the possible peptide fragments containing disulfide bonds in the cleavage products by using the F-LINK program. In the present study, there were 22 distinguishable disulfide-containing peptide fragments (Table 2).

There are 105 possible permutations of four disulfide bonds possible in the SMB domain. However, as indicated below, the active rVN1−51 peptide is expected to contain the Cys^{25}−Cys^{31} disulfide bond, which reduced the number of combinatorially possible configurations to 15. Evidence for the presence of the Cys^{25}−Cys^{31} disulfide bond in active VN1−51 is provided by the apparent requirement for this bond to be intact for binding to mAb 153 during purification (*34*). Anti-VN mAb 153 recognizes a conformation-dependent immunoepitope within the SMB domain (*38*), and the recognition site appears to be in close proximity to the PAI-1 binding site, presumably in the central region (i.e., between residues 16−34) of the domain (*32*). This epitope was further mapped by determining whether a synthetic peptide containing this region was also recognized by mAb 153 (Figure 7A). The peptide (VN22−31, $Asp^{22}Glu^{23}Leu^{24}Cys^{25}Ser^{26}$-$Tyr^{27}Tyr^{28}Gln^{29}Ser^{30}Cys^{31}$) could be purified by affinity chromatography on a mAb 153 affinity column, demonstrating that it contains the epitope. The peptide purified in this way represents less than 3% of the total peptide applied to the column, indicating the specificity of the purification and suggesting that the majority of the peptide in the preparation was incorrectly synthesized or misfolded. The material that eluted from the column had a molecular mass of 1207 Da, consistent with the calculated mass of a monomeric peptide containing a single disulfide bond (i.e., Cys^{25}−Cys^{31}). The molecular mass increased to 1209 Da upon reduction, consistent with this conclusion. Figure 7A shows that the oxidized peptide competes with mAb 153 for binding to

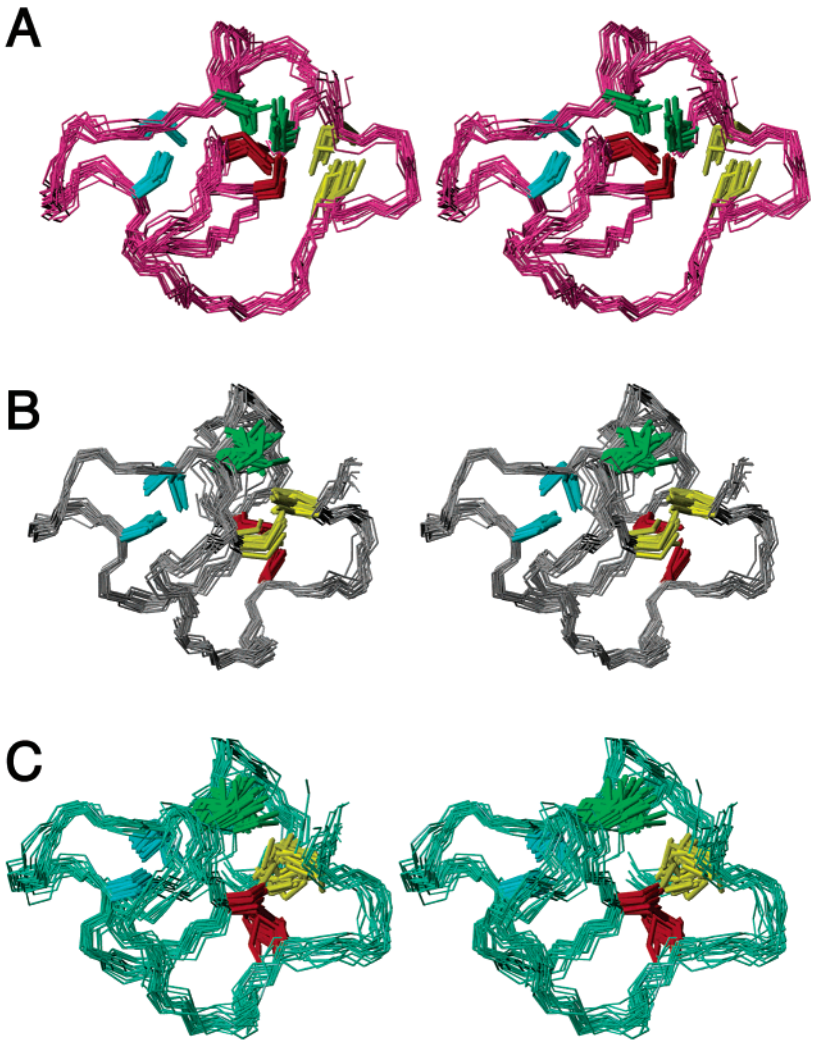

FIGURE 5: Calculated solution structures of rVN1−51. Only the ordered residues, 4−39, are shown, and the families are superimposed on the backbone of residues 4−39. (A) Stereoview of a superposition of 20 structures calculated with the 509 disulfide bond arrangement. The structures were superimposed on the backbone of residues 4−39. Backbone is shown in pink, the side chains of Cys^{5} and Cys^{9} are in yellow, Cys^{19} and Cys^{21} are in red, Cys^{25} and Cys^{31} are in cyan, and Cys^{32} and Cys^{39} are in green. (B) Stereoview of a superposition of 20 structures calculated with the 521 disulfide bond arrangement. Backbone is shown in gray, the side chains of Cys^{5} and Cys^{21} in yellow, Cys^{19} and Cys^{32} in green, Cys^{25} and Cys^{31} in cyan and Cys^{9} and Cys^{39} in red. (C) Stereoview of a superposition of 20 structures calculated with the 539 disulfide bond arrangement. Backbone is shown in cyan, the side chains of Cys^{5} and Cys^{39} in yellow, Cys^{19} and Cys^{32} in green, Cys^{25} and Cys^{31} in cyan and Cys^{9} and Cys^{39} in red.

immobilized VN, but that the reduced peptide does not. The oxidized peptide also competes with PAI-1 for binding to immobilized VN (data not shown). Taken together, these results indicate that mAb 153 recognizes and binds to the conformation-dependent epitope created by residues 22−31 of the SMB domain when it is stabilized by the formation of the Cys^{25}−Cys^{31} disulfide bond, but does not recognize this epitope when the Cys^{25}−Cys^{31} bond is reduced.

On the basis of the above discussion, we considered only the 15 combinatorially possible disulfide linkage patterns that include the Cys^{25}−Cys^{31} bond in our acid fragmentation studies. The observed fragments were matched to one or more of the 15 possible disulfide patterns. A mismatch, where the mass of an observed fragment does not match any of the possible fragments from a given disulfide arrangement, provides evidence that other disulfide bond arrangements are more probable. The results from the F-LINK program, matching possible fragments from all 15 possible disulfide bond arrangements with the masses of the observed fragments, are presented in Table 2. A "+" in the table indicates that the particular disulfide bond arrangement is compatible with the observation of a particular fragment. A "−" indicates that the program was unable to assign a disulfide-bonded fragment to a particular arrangement that would be consistent with the observed mass, and thus represents a "mismatch". The total number of mismatches for each disulfide bond arrangement appears as the last row of the table. The lowest number of mismatches are observed for the disulfide bond pattern 509, indicating that this arrangement is the most probable. The results for the disulfide bond arrangement 509 are presented in column 1 of Table 2, and show only two mismatches, compared to 8 (column 2) and 11 (column 3) mismatches, respectively, for the disulfide bond arrangements 521 and 539.

The F-LINK program was able to unambiguously define the disulfide bonds contained in three of the acid-cleavage products (606.8, 687.8, and 859.7 Da), taking into account the binding epitope in the SMB domain for anti-VN mAb 153, which requires the Cys^{25}−Cys^{31} disulfide bond. The results for these fragments are highlighted in Table 2.

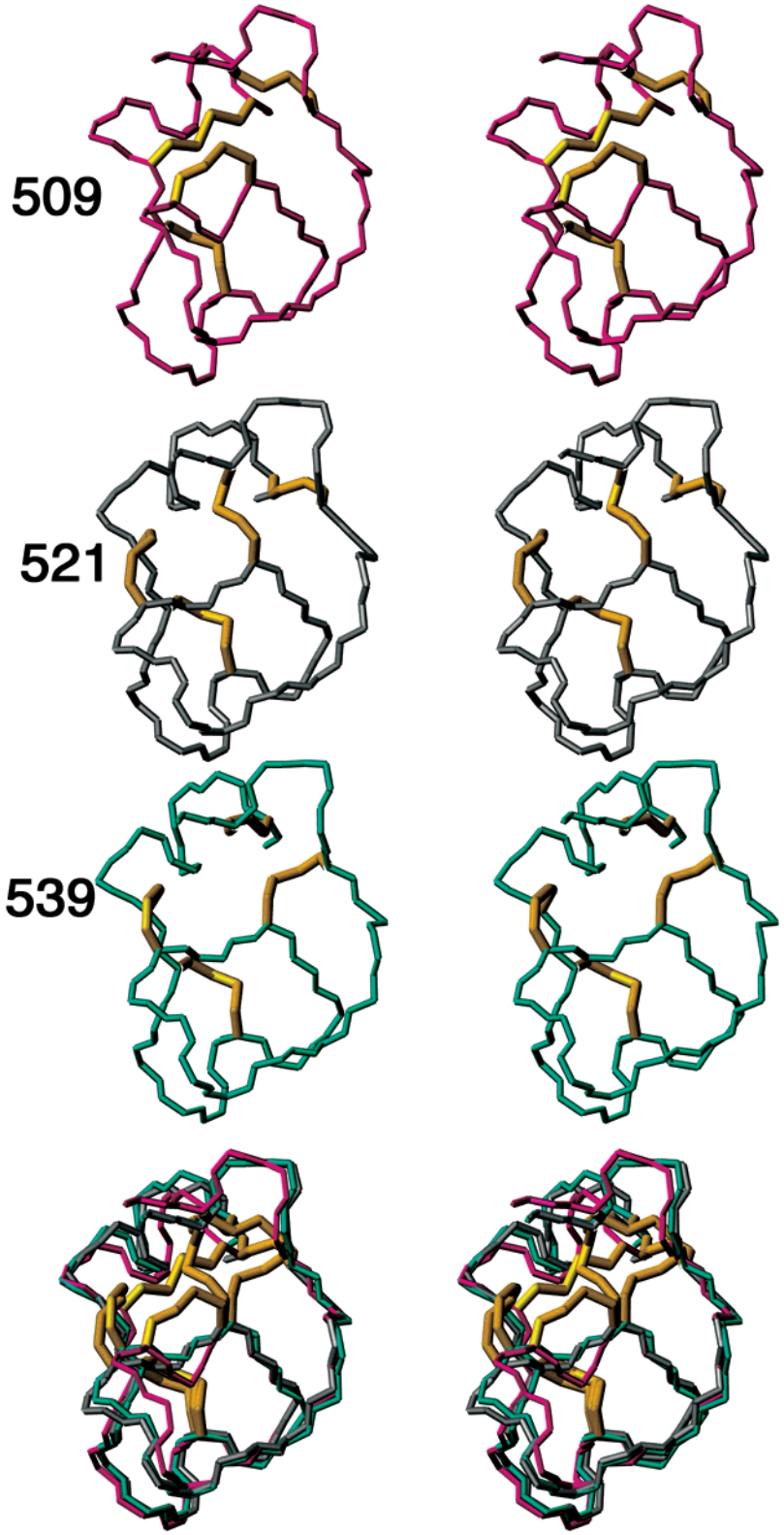

FIGURE 6: Stereopairs of the backbone of a representative member of the structure family obtained with the 509 (pink), the 521 (gray), and 539 (blue) disulfide arrangements, shown separately as indicated and also superimposed (bottom) on the backbone between residues 4 and 40.

Interestingly, the presence of these three fragments was incompatible with most of the suggested disulfide arrangements. Only disulfide bond arrangement 509 can account for all of these fragments. Suggested structures for these fragments, together with their disulfide connectivities, are shown in Table 3. The analysis showed no fragments among the 22 that were unique for the 521 or 539 structures. Taken together, these data provide strong evidence that the majority of the rVN1−51 in this sample has the uncrossed linear disulfide bond pattern.

Experimental Demonstration of Alternative Disulfide Arrangements. To determine experimentally whether the disulfide bond arrangement of the SMB domain may vary without affecting the PAI-1 binding activity, we prepared

Table 2: Assignment of Cleavage Products from Partial Acid Hydrolysis of rVN1−51 to 15 Possible Disulfide Bond Arrangements[a]

Cleavage	1(509)	2(521)	3(539)	4	5	6	7	8	9	10	11	12	13	14	15
Product	5-9	5-21	5-39	5-9	5-9	5-19	5-19	5-19	5-21	5-21	5-32	5-32	5-32	5-39	5-39
Observed	19-21	9-39	9-21	19-32	19-39	9-21	9-32	9-39	9-19	9-32	9-19	9-21	9-39	9-19	9-32
Mass (Da)	32-39	19-32	19-32	21-39	21-32	32-39	21-39	21-32	32-39	19-39	21-39	19-39	19-21	21-32	19-21
453.3	+	+	+	+	+	+	+	+	+	+	+	+	+	+	+
470.9	+	+	+	+	+	+	+	+	+	+	+	+	+	+	+
512.0	+	+	+	+	+	+	+	+	+	+	+	+	+	+	+
513.0	+	+	+	+	+	+	+	+	+	+	+	+	+	+	+
527.8	+	+	+	+	+	+	+	+	+	+	+	+	+	+	+
541.0	+	+	–	+	+	–	–	–	+	+	–	–	–	–	–
549.8	+	+	+	+	+	+	+	+	+	+	+	+	+	+	+
581.9	+	+	+	+	+	+	+	+	+	+	+	+	+	+	+
598.4	+	+	+	+	+	+	–	+	+	–	+	+	+	+	–
606.8	+	–	–	–	–	–	–	–	–	–	–	–	+	–	+
625.8	+	+	+	+	+	+	+	+	+	+	+	+	+	+	+
685.8	+	–	–	+	+	–	+	–	–	+	+	+	+	–	+
687.8	+	–	–	–	–	+	–	–	+	–	–	–	–	–	–
727.9	–	+	–	–	–	–	+	+	–	+	+	+	+	–	+
742.9	+	–	–	+	+	–	+	–	–	+	+	+	+	–	+
743.9	+	–	–	+	+	–	+	–	–	+	–	–	–	–	+
783.7	–	+	+	–	–	–	+	–	+	+	+	–	–	+	+
814.9	+	+	–	+	+	–	–	–	+	+	–	–	–	–	–
853.7	+	+	+	+	+	+	+	+	+	+	+	+	+	+	+
859.7	+	–	–	+	+	–	–	–	–	–	–	–	–	–	–
871.9	+	–	–	+	+	–	–	–	–	–	+	+	+	–	–
876.8	+	–	–	–	–	+	–	–	+	–	–	–	–	–	–
Number of mismatches	2	8	11	5	5	10	8	11	7	6	7	8	7	11	7

[a] rVN1−51 cleavage products (total of 22) containing disulfide bonds were analyzed using the F-LINK program. The total number of times that each theoretical disulfide arrangement (a total of 15 possible arrangements containing the Cys25−Cys31 disulfide bond) was inconsistent with the presence of an observed cleavage product ("−" in the table) is shown in the bottom line. A "+" in the table indicates that the theoretical mass of a fragment matches the observed mass. The rows for the three fragments that show a preference for the disulfide arrangement 509 are shaded. Disulfide bond arrangements 509 (column 1), 521 (column 2), and 539 (column 3) are outlined with a heavy box.

an SMB mutant (rVN1−51Asn^{14} → Met), in which Asn^{14} was replaced by Met. If the linear uncrossed disulfide arrangement was present exclusively in the recombinant 1−97 fragment, then CNBr cleavage of the Asn^{14} → Met mutant should result in two fragments, cleaved at Met^{51} and at Met^{14}, with no disulfide connections between the N- and C-terminal fragments. However, analysis of the CNBr-treated sample (Table 4) revealed a single fragment with a molecular mass of 5749 Da (i.e., approximately the same as that expected for the intact 1−51 fragment). Reduction of rVN1−51Asn^{14} → Met with DTT resulted in the generation of two fragments of molecular mass 4213 and 1542 Da (Table 4). These are the masses expected after cleavage at residue 14. These results indicate that rVN1−51Asn^{14} → Met is held together by disulfide bonds between the smaller 1−14 fragment and the larger 15−51 fragment. Despite this, rVN1−51Asn^{14} → Met has the same PAI-1 binding activity as rVN1−51 (Figure 7B) and binds to a column conjugated with an anti-VN mAb (mAb 153) (data not shown). The connection of residues 1−14 in rVN1−51Asn^{14} → Met to residues 15−51 by disulfide linkages is incompatible with the results obtained for the wild-type rVN1−51, which indicate that residues 5 and 9 are disulfide bonded to each other. Both wild-type and mutant proteins have an intact 25−

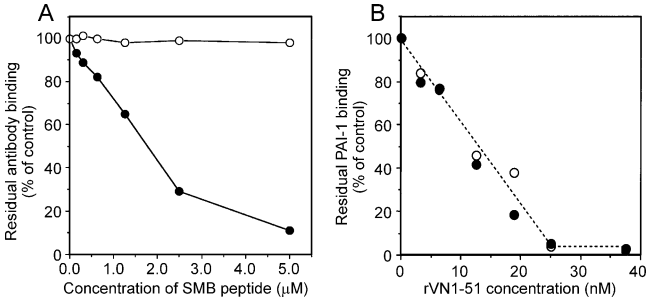

FIGURE 7: (A) Competitive surface plasmon resonance analysis (BIAcore) using the synthetic SMB peptide $Asp^{22}Glu^{23}Leu^{24}$-$Cys^{25}Ser^{26}Tyr^{27}Tyr^{28}Gln^{29}Ser^{30}Cys^{31}$ (VN22−31) to determine the immunoepitope in the SMB domain for anti-VN mAb 153 binding. Urea-activated VN was immobilized on the sensor chips, and then anti-VN mAb 153 samples, previously incubated with increasing concentrations of the oxidized (closed circles) or reduced (open circles) synthetic peptide, were injected onto the chips. The amount of residual mAb binding activity was then determined. (B) Binding activity of rVN1−51Asn^{14} → Met to PAI-1, determined by competitive BIAcore assay. PAI-1 samples (25 nM), incubated with increasing concentrations of rVN1−51Asn^{14} → Met (closed circles) and rVN1−51 (open circles), were injected onto a chip containing immobilized urea-activated VN.

Table 3: Unique Cleavage Products of rVN1−51[a]

rVN1−51 cleavage product (obsd mass, Da)	predicted rVN1−51 cleavage product (calculated mass, Da)	disulfide connectivity
product 1 (606.8)	$K^{17}K^{18}C^{19}Q^{20}C^{21}$ (606.8)	$Cys^{19}-Cys^{21}$
product 2 (687.8)	$C^{25}C^{31}C^{32}C^{39}K^{40}P^{41}$ (687.9)	$Cys^{25}-Cys^{31}$ $Cys^{32}-Cys^{39}$
product 3 (859.7)	$C^{5}K^{6}G^{7}C^{9}T^{10}E^{11}G^{12}F^{13}$ (860.0)	$Cys^{5}-Cys^{9}$

[a] Three rVN1−51 cleavage products, unique for the uncrossed disulfide bond arrangement 509, were identified by the F-LINK software program.

Table 4: Masses of Peptides after CNBr Hydrolysis

	before reduction		after reduction	predicted peptide	
	obsd mass (Da)	calc mass (Da)	obsd mass (Da)	residues	calcd mass (Da)
rVN1−51	5763	5762	5775[a]	1−51	5770
rVN1−51 Asn^{14} → Met	5749	5750	4213[b]	15−51	4215
			1542[b]	1−14	1543

[a] Reduced by 10 mM DTT in 10 mM tris buffer, pH 7.4 at 45° for 1 h. [b] Reduced by 100 mM DTT in 10 mM tris buffer, pH 7.4 at room temperature for 1 h.

31 disulfide bond, since both bind to PAI-1 and to mAb 153. The unimpaired PAI-1 binding activity of the mutant rVN1−51Asn^{14} → Met indicates that the disulfide bonding arrangement apart from the 25−31 bond may be less important for PAI-1 binding activity, and that several arrangements can be accommodated.

Results of Conformational Energy Calculations. Conformational energy calculations were performed using a total of five different disulfide bond arrangements, shown in Figure 2. The 509 arrangement is the one suggested by the chemical studies (*34* and the present work). The 521 and 539 arrangements were suggested by the NMR structure calculations without added disulfide bond restraints. The 532 arrangement is another alternative that preserves both the $Cys^{19}-Cys^{21}$ and $Cys^{25}-Cys^{31}$ disulfides. The 509′ structure was suggested by the adjacent positions of Cys^{31} and Cys^{32} as a possible variant of the strictly linear 509 arrangement. Of these arrangements, only the 509′ arrangement does not contain the $Cys^{25}-Cys^{31}$ disulfide. All five disulfide bond arrangements were compatible with the UNRES/CSA conformational studies.

Table 5: Relative Average Energies (kcal/mol) (Averaged over the MD Trajectory), for Different Disulfide Arrangements, for Restrained and Unrestrained MD Runs

relative average energy	disulfide bond arrangement				
	509	509′	539	521	532
restrained MD	36	109	20	0	0
unrestrained MD	43	nd[a]	11	0	31

[a] nd − not determined.

Following model-building of the different disulfide-bonded structures from the backbone coordinates of the X-ray crystal structure (*37*), the relative energy of each disulfide bond arrangement was assessed following 1-ns molecular dynamics calculations. Two sets of molecular dynamics calculations were carried out, one using a set of 650 NMR restraints and the other unrestrained. In the restrained calculations, the average structures (averaged over the molecular dynamics trajectories) for all models except 509′ were very similar to the X-ray structure (RMSD for the C^{α} atoms smaller than 2.3 Å). The 509′ structure drifted more from the X-ray structure, with an RMSD of 3.6 Å. The average RMSDs from the NMR distance restraints were less than 0.02 Å for all models except 509′, for which the RMSD was 0.04 Å. In general, all structures satisfy the NMR restraints very well. The relative average energies are given in Table 5. Given the energy fluctuations of ∼16 kcal/mol during a molecular dynamics run, it appears that all disulfide arrangements except 509′ are feasible ones for the molecule in solution. Analysis of the C−S−S−C dihedral angles also supports the above conclusion. Table 6 contains values of each of the four disulfide dihedral angles, which may be compared to the favorable values of ±90°. Model 509′ exhibits significantly larger deviations than those found for the other models. On the basis of the above results, model 509′ can be eliminated from further consideration.

The results of the unrestrained molecular dynamics calculations without using NMR restraints (and excluding 509′) are also shown in Tables 5 and 6. They are consistent with those from restrained molecular dynamics. All four remaining models are, therefore, possible disulfide bond arrangements, with model 509 being somewhat less likely than the others by these criteria. The average disulfide bond torsion angles (Table 6) are generally within a few degrees of the preferred values of 90° and −90°.

DISCUSSION

PAI-1 belongs to the serpin superfamily, of which the best characterized members are serine protease inhibitors implicated in various biological processes such as inflammation, blood coagulation, and fibrinolysis. However, unlike other serpins, PAI-1 undergoes a rapid, dramatic conformational change in solution, where the active ("stressed") form is

Table 6: Values of the C−S−S−C Dihedral Angle [dih, deg] (Averaged over the MD Trajectory) for Each of Four Disulfide Bonds, for Restrained and Unrestrained MD Runs

	509		509′		521		532		539	
	bond	dih	bond	dih	bond	dih	bond	dih	bond	dih
restrained MD	5-9	137	5-9	−169	5-21	−77	5-32	70	5-39	−92
	19-21	106	19-21	8	9-39	−77	9-39	−81	9-21	−83
	25-31	92	25-32	−101	19-32	88	19-21	78	19-32	84
	32-39	99	31-39	−154	25-31	87	25-31	87	25-31	87
unrestrained MD	5-9	94		nd[a]	5-21	−104	5-32	73	5-39	−89
	19-21	73		nd	9-39	−80	9-39	−79	9-21	−99
	25-31	95		nd	19-32	93	19-21	76	19-32	88
	32-39	125		nd	25-31	100	25-31	91	25-31	94

[a] nd − not determined.

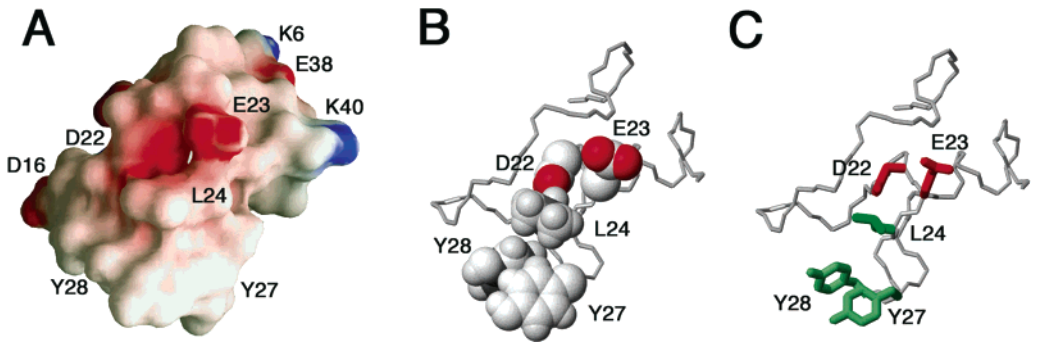

FIGURE 8: (A) Surface representation of a single structure of the SMB domain containing the 521 disulfide bond arrangement, with an electrostatic surface calculated using the program GRASP (*60*). The hydrophobic surface comprising Leu[24], Tyr[27], and Tyr[28] can be clearly seen at the bottom of the picture, with the conserved acidic residues Asp[22] and Glu[23] forming a concentrated area of negative charge in the center. (B, C) MOLMOL (*59*) representations of the same structure, in the same orientation as panel A, illustrating the position of the side chains of the putative binding surface.

converted into the inactive ("relaxed" or latent) form by the insertion of the reactive center loop as strand 4 between strands 3 and 5 of the central β-sheet of the molecule (*70*−*72*). Only the stressed form of PAI-1 binds to the SMB domain, an interaction that delays the latency transition of PAI-1 and stabilizes the inhibitor. Previous mutational studies (*35*, *38*) suggested that residues 24−28 in the SMB domain of VN interact with PAI-1.

The studies in this report demonstrate that the three-dimensional structure of the SMB domain is extremely compact and that the disulfide bonds are packed in the center of the domain forming a covalently bonded core (Figures 5 and 6). The amino acid composition of the folded part of the domain (residues 4−39) shows, in addition to the eight Cys residues that comprise the disulfides, a preponderance of hydrophilic residues: 8 acidic, 5 basic, and 10 neutral. Only 6 of the 37 residues in the SMB domain (Phe[13], Val[15], Leu[24], Tyr[27], Tyr[28], and Tyr[35]) can be considered to have hydrophobic side chains. All of these side chains are clustered in one region on the surface of the SMB domain, surrounded by surface hydrophilic residues, with a prominent acidic patch at residues Asp[22] and Glu[23] (Figure 8). Figure 9 shows some of the NMR evidence for close contacts between these hydrophobic side chains: nuclear Overhauser effect (NOE) connectivities (shown boxed in Figure 9) are visible in the spectrum between the side chains of Leu[24] and Val[15] and those of the aromatic rings of Phe[13], Tyr[27], and Tyr[28].

With the exception of Val[15], these amino acid residues are conserved between human, rabbit, mouse, and pig VN sequences, all of which bind tightly to PAI-1. Figure 10 shows the sequence alignment of the SMB domains of these VN species, together with the relevant sequences of several other proteins that contain SMB-like domains (*35*). None of these SMB homologues binds to PAI-1 (*35*); Leu[24], Tyr[27], and Tyr[28], which have been shown by mutagenesis to be absolutely required for PAI-1 binding (*35*, *38*), and which appear in our structure as a group on the surface of the domain (Figure 8), are not conserved in any of the nonfunctional SMB-domain homologues (Figure 10). The three-dimensional structure of the SMB domain thus implies that its high-affinity interaction with PAI-1 results from the capacity of the disulfide bonded domain to present a hydrophobic binding surface to the inhibitor. The covalently bonded disulfide core would appear to be absolutely necessary for the correct interaction to occur, as proteins that contain less stable noncovalent hydrophobic cores would perhaps be in danger of unfolding/misfolding and mixing up the hydrophobic groups. The hydrophobic side chains are clearly arranged in a highly specific way on the surface of the SMB domain.

Other highly conserved residues in the PAI-1-binding SMB domains include Asp[22] and Glu[23]. These residues are also present on the surface of the SMB domain, forming a negatively charged patch on one side of the hydrophobic patch. This arrangement most likely gives additional specificity to the interaction. The alanine scanning mutagenesis study (*35*) demonstrated that Asp[22] is critical for PAI-1 binding and is required to stabilize PAI-1 activity. Although Glu[23] does not seem to be required for PAI-1 binding, it plays an important role in uPAR binding (*8*). Again, both Asp[22] and Glu[23] are conserved in VN molecules that bind PAI-1 but not in the nonbinding SMB homologues (Figure 10).

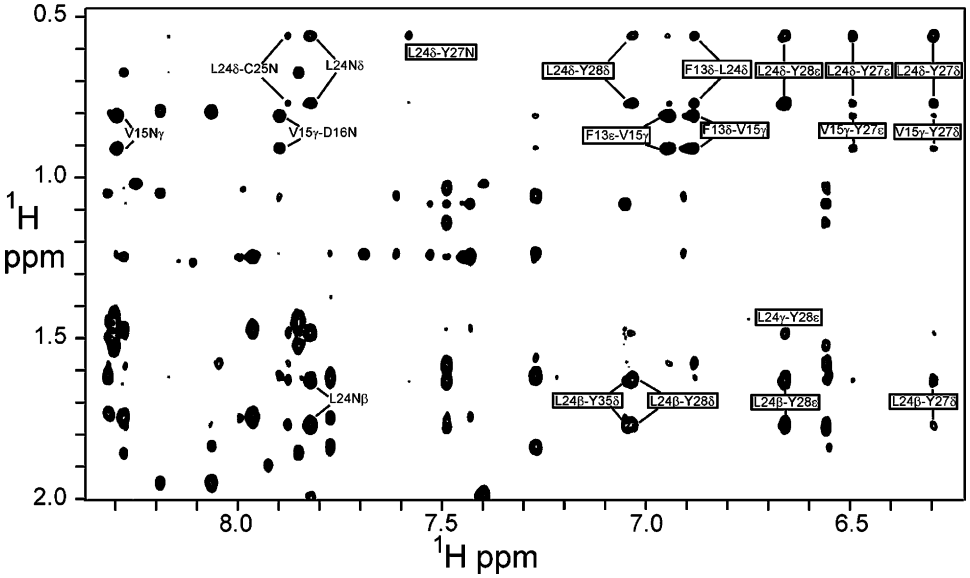

FIGURE 9: Portion of the 900 MHz 2D NOESY spectrum of the SMB domain, showing NOEs between aliphatic protons and aromatic/amide protons. The connectivities labeled are those between the side chains of the hydrophobic patch. Boxed labels indicate NOEs between nonadjacent side chains.

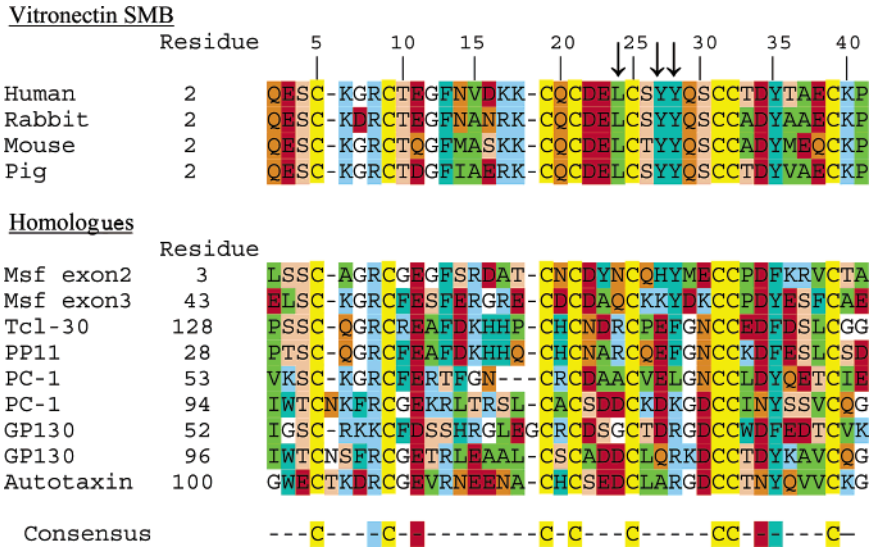

FIGURE 10: Sequence alignment of SMB domains present in vitronectin from different species, and in the indicated SMB-like domains (homologues): Msf, megakaryocyte-stimulating factor; Tcl-30, T cell-specific protein; PP11, placental-specific protein 11; PC-1, plasma cell membrane glycoprotein; GP-130, tumor cell surface antigen (*35*). Amino acid types are identified by colors: green, hydrophobic (A, V, L, I, P, M); blue-green, aromatic (F, Y, W, H); yellow, cysteine; red, acidic (D, E); blue, basic (K,R); orange, carboxamide (N, Q); tan, hydrophilic (S, T); white, glycine. Arrows indicate the positions of Leu^{24}, Tyr^{27}, and Tyr^{28}. All of the homologue domains were identified on the basis of the positions of the eight Cys residues, shown as a consensus at the bottom of the figure. In addition, there are four other positions with close homology between the SMB domains and the SMB-like domains: a basic amino acid (R, K) immediately before the Cys at position 9 of SMB, an acidic residue (E, D) in the position corresponding to residue 11 of SMB, an Asp or Asn residue corresponding to Asp^{34} of SMB, and an aromatic residue (Y or F) corresponding to Tyr^{35}.

The hydrophobic patch is not excessively hydrophobic, and many of the component side chains could be thought of as partly hydrophilic. For example, Tyr^{27} and Tyr^{28} contain the ζ-hydroxyl group on the aromatic ring. Nevertheless, electrostatic calculations with the program GRASP (*60*), illustrated in Figure 8, indicate a prominent hydrophobic patch in the vicinity of the two adjacent tyrosines (Tyr^{27} and Tyr^{28}), with a well-defined acidic patch to one side, constituted by the adjacent Asp^{22} and Glu^{23} side chains. The occurrence on the surface of the SMB domain of bulky, largely hydrophobic side chains which also contain functional groups capable of favorable interactions with water may reflect the necessity for the hydrophobic patch to remain solvent exposed to initiate binding—if the patch was uniformly and deeply hydrophobic, it might cause the VN molecules to aggregate in solution or to bind to other molecules nonspecifically.

After completion of our NMR solution structure calculations, Zhou et al. (*37*) reported the X-ray crystal structure of the complex between the SMB domain and PAI-1. The binding interface between the SMB domain and PAI-1 is consistent with the mutagenesis data for VN (*35*, *38*) and PAI-1 (*15*, *73*−*75*) and with our NMR-derived solution structure showing the functional residues of the SMB domain in a contiguous patch on the surface (Figure 8). The backbone fold of the X-ray structure is quite consistent with the family

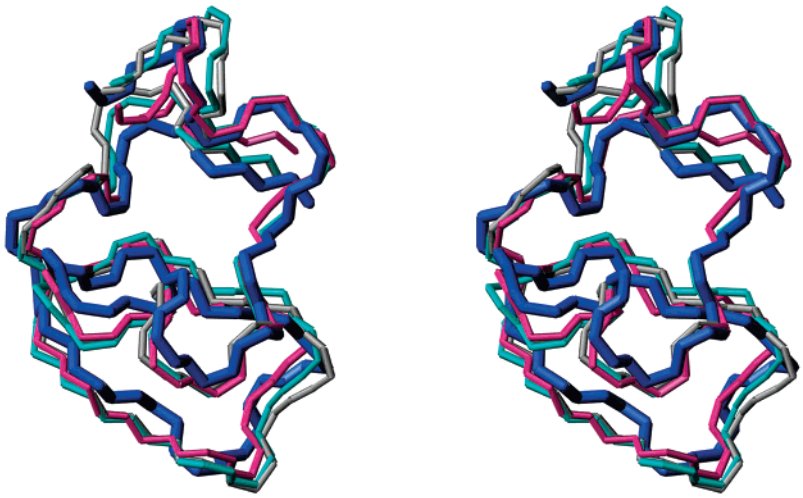

FIGURE 11: Stereoview of a superposition of single structures of the SMB domain with disulfide arrangements 509 (pink), 521 (gray), and 539 (cyan) with that obtained from the X-ray structure of the SMB−PAI-1 complex (1OCO) (*37*) (blue).

of NMR structures in solution, no matter what the disulfide arrangement (Figure 11). The all-atom RMSDs between the X-ray and the average NMR structures are 1.64, 1.64, and 1.72 Å, for models 509, 521, 539, respectively. Thus, the nature of the PAI-1 binding site, the major issue as far as the structure of the SMB domain is concerned, is completely consistent between the bound SMB domain in the crystal and the free SMB domain in solution.

The difference in the disulfide bond arrangement between the published chemical analysis (*34*) and the X-ray structure (*37*) was unexpected. The disulfide bond arrangement determined in the X-ray crystal structure is the same as that in the disulfide arrangement 521 (Figure 2). Since the NMR spectra do not report directly on disulfide bonds, there remains some ambiguity in the solution structures of the free SMB domain with regard to the disulfide arrangement. Chemical studies described herein and in ref *34* implicate the linear uncrossed arrangement 509, while the comparable overall energies of the various calculated structures appear to indicate that a number of different disulfide arrangements are possible. The conformational energy calculations show that the only significant difference between the structure families with the disulfide bond arrangements shown in Figure 2 is an energy disadvantage for the crossed form 509′.

The presence of at least two alternative disulfide arrangements that remain compatible with PAI-1 binding is shown by the results obtained for the rVN1−51Asn^{14} → Met mutant protein (Figure 7B; Table 4). The present work does not delineate the disulfide bond arrangement in this SMB mutant, but it is clear from Table 4 that the disulfide bond arrangement in this mutant differs from the linear uncrossed pattern observed for the wild-type protein, and that the Cys^5−Cys^9 disulfide is not present in the majority of the protein molecules under these conditions. The binding experiments with anti-VN mAb 153 and PAI-1 indicate that the mutant protein contains the required Cys^{25}−Cys^{31} disulfide bond.

The purpose of the present study was to clarify the disulfide bond arrangement and 3-D structure of the active SMB domain that contains high-affinity binding sites for PAI-1 and the anti-VN monoclonal antibody 153. It should be pointed out that the high-affinity binding site for PAI-1 is cryptic in native VN and is exposed only upon treatment of native VN with denaturants such as urea, suggesting that the native SMB domain normally lacks the high-affinity binding site for PAI-1 (*32*). Our highly purified rVN1−51 contained a high-affinity binding site for PAI-1, and its binding affinity was the same as that for the SMB domain prepared from urea-activated VN (data not shown). However, we do not know whether there is actual variability and plasticity of the disulfide bond arrangement in the native SMB domain since neither the disulfide bond arrangement nor the structure of the SMB domain within native VN has been determined. In addition, it is possible that our rVN1−51 and rVN1−51Asn^{14} → Met represent scrambled intermediate isomers of the native SMB domain generated during biosynthesis in bacteria and/or during the purification procedure, thereby resulting in an altered disulfide bond arrangement in the recombinant molecule, which nevertheless retains full biological activity. These issues cannot be resolved until the folding process, as well as the disulfide bond arrangement and structure, have been determined for the native SMB domain. Until then, we propose that the potential for variability and/or plasticity of the disulfide bond arrangement of the SMB domain may have relevance in the design of inhibitors for the physiological partners of vitronectin.

CONCLUSIONS

The structure of the recombinant SMB domain free in solution contains a core of four disulfide bonds which can be arranged in several ways, including a previously published sequential arrangement (*34*), and still allow consistency of the structure with the NMR data and comparable conformational energies. The recent report of the X-ray structure of the SMB domain in a complex with PAI-1 (*37*) is quite consistent with the backbone fold and PAI-1 binding surface inferred from the solution NMR spectra of the free protein. Whether the difference in disulfide arrangement seen in the PAI-1 complex compared to that determined for free SMB in the chemical mapping experiments (*34* and present paper) will prove to be significant for the function of VN is a subject for further study. The X-ray structure of SMB in the complex and the NMR structure of the free domain in solution are very similar in the local structure of the principal PAI-1 binding loop and are consistent with previous mutagenesis

studies (*35*, *38*). This loop, delimited by the $Cys^{25}-Cys^{31}$ disulfide bond, appears to present a binding surface for PAI-1 and uPAR via exposed conserved hydrophobic side chains of Leu^{24}, Tyr^{27}, and Tyr^{28} and the nearby acidic side chains of Asp^{22} and Glu^{23}. The biochemical, structural, and computational evidence summarized in this paper points to the possibility of heterogeneity or variability in the disulfide arrangement of the SMB domain. We conclude that a variety of allowed disulfide bond arrangements in the SMB domain may be compatible with biological activity, as long as the $Cys^{25}-Cys^{31}$ disulfide bond is preserved.

ACKNOWLEDGMENT

We thank John Chung for helpful comments on the NMR spectroscopy, Elizabeth Getzoff and John Tainer for comments on the structure determination, and Peter Wright for continuing helpful discussions.

REFERENCES

1. Tomasini, B. R., and Mosher, D. F. (1991) in *Progress in Hemostasis and Thrombosis* (Coller, B. S., Ed.) pp 269−305, Saunders, Philadelphia.
2. Preissner, K. T., and Seiffert, D. (1998) Role of vitronectin and its receptors in haemostasis and vascular remodeling, *Thromb. Res. 89*, 1−21.
3. Brooks, P. C., Clark, R. A., and Cheresh, D. A. (1994) Requirement of vascular integrin alpha v beta 3 for angiogenesis, *Science 264*, 569−571.
4. Seiffert, D., and Smith, J. W. (1997) The cell adhesion domain in plasma vitronectin is cryptic, *J. Biol. Chem. 272*, 13705−13710.
5. Smith, J. W., Vestal, D. J., Irwin, S. V., Burke, T. A., and Cheresh, D. A. (1990) Purification and functional characterization of integrin alpha v beta 5. An adhesion receptor for vitronectin, *J. Biol. Chem. 265*, 11008−11013.
6. Waltz, D. A., and Chapman, H. A. (1994) Reversible cellular adhesion to vitronectin linked to urokinase receptor occupancy, *J. Biol. Chem. 269*, 14746−14750.
7. Wei, Y., Waltz, D. A., Rao, N., Drummond, R. J., Rosenberg, S., and Chapman, H. A. (1994) Identification of the urokinase receptor as an adhesion receptor for vitronectin, *J. Biol. Chem. 269*, 32380−32388.
8. Deng, G., Curriden, S. A., Wang, S., Rosenberg, S., and Loskutoff, D. J. (1996) Is plasminogen activator inhibitor-1 the molecular switch that governs urokinase receptor-mediated cell adhesion and release? *J. Cell Biol. 134*, 1563−1571.
9. Sidenius, N., and Blasi, F. (2000) Domain 1 of the urokinase receptor (uPAR) is required for uPAR-mediated cell binding to vitronectin, *FEBS Lett. 470*, 40−46.
10. Declerck, P. J., De Mol, M., Alessi, M. C., Baudner, S., Paques, E. P., Preissner, K. T., Muller-Berghaus, G., and Collen, D. (1988) Purification and characterization of a plasminogen activator inhibitor 1 binding protein from human plasma. Identification as a multimeric form of S protein (vitronectin), *J. Biol. Chem. 263*, 15454−15461.
11. Wiman, B., Almquist, A., Sigurdardottir, O., and Lindahl, T. (1988) Plasminogen activator inhibitor 1 (PAI) is bound to vitronectin in plasma, *FEBS Lett. 242*, 125−128.
12. Mimuro, J., and Loskutoff, D. J. (1989) Purification of a protein from bovine plasma that binds to type 1 plasminogen activator inhibitor and prevents its interaction with extracellular matrix. Evidence that the protein is vitronectin, *J. Biol. Chem. 264*, 936−939.
13. Salonen, E. M., Vaheri, A., Pollanen, J., Stephens, R., Andreasen, P., Mayer, M., Dano, K., Gailit, J., and Ruoslahti, E. (1989) Interaction of plasminogen activator inhibitor (PAI-1) with vitronectin, *J. Biol. Chem. 264*, 6339−6343.
14. Gibson, A., Baburaj, K., Day, D. E., Verhamme, I., Shore, J. D., and Peterson, C. B. (1997) The use of fluorescent probes to characterize conformational changes in the interaction between vitronectin and plasminogen activator inhibitor-1, *J. Biol. Chem. 272*, 5112−5121.
15. Lawrence, D. A., Berkenpas, M. B., Palaniappan, S., and Ginsburg, D. (1994) Localization of vitronectin binding domain in plasminogen activator inhibitor-1, *J. Biol. Chem. 269*, 15223−15228.
16. Wiman, B., Lindahl, T., and Almqvist, A. (1988) Evidence for a discrete binding protein of plasminogen activator inhibitor in plasma, *Thromb. Haemostasis 59*, 392−395.
17. Podor, T. J., Peterson, C. B., Lawrence, D. A., Stefansson, S., Shaughnessy, S. G., Foulon, D. M., Butcher, M., and Weitz, J. I. (2000) Type 1 plasminogen activator inhibitor binds to fibrin via vitronectin, *J. Biol. Chem. 275*, 19788−19794.
18. Wiman, B. (1995) Plasminogen activator inhibitor 1 (PAI-1) in plasma: its role in thrombotic disease, *Thromb. Haemostasis 74*, 71−76.
19. Andreasen, P. A., Egelund, R., and Petersen, H. H. (2000) The plasminogen activation system in tumor growth, invasion, and metastasis, *Cell Mol. Life Sci. 57*, 25−40.
20. Foekens, J. A., Peters, H. A., Look, M. P., Portengen, H., Schmitt, M., Kramer, M. D., Brunner, N., Janicke, F., Meijer-van Gelder, M. E., Henzen-Logmans, S. C., van Putten, W. L., and Klijn, J. G. (2000) The urokinase system of plasminogen activation and prognosis in 2780 breast cancer patients, *Cancer Res. 60*, 636−643.
21. Deng, G., Curriden, S. A., Hu, G., Czekay, R. P., and Loskutoff, D. J. (2001) Plasminogen activator inhibitor-1 regulates cell adhesion by binding to the somatomedin B domain of vitronectin, *J. Cell Physiol. 189*, 23−33.
22. Stefansson, S., and Lawrence, D. A. (1996) The serpin PAI-1 inhibits cell migration by blocking integrin alpha V beta 3 binding to vitronectin, *Nature 383*, 441−443.
23. Kjoller, L., Kanse, S. M., Kirkegaard, T., Rodenburg, K. W., Ronne, E., Goodman, S. L., Preissner, K. T., Ossowski, L., and Andreasen, P. A. (1997) Plasminogen activator inhibitor-1 represses integrin- and vitronectin-mediated cell migration independently of its function as an inhibitor of plasminogen activation, *Exp. Cell Res. 232*, 420−429.
24. Czekay, R. P., Aertgeerts, K., Curriden, S. A., and Loskutoff, D. J. (2003) Plasminogen activator inhibitor-1 detaches cells from extracellular matrices by inactivating integrins, *J. Cell Biol. 160*, 781−791.
25. Suzuki, S., Pierschbacher, M. D., Hayman, E. G., Nguyen, K., Ohgren, Y., and Ruoslahti, E. (1984) Domain structure of vitronectin. Alignment of active sites, *J. Biol. Chem. 259*, 15307−15314.
26. Fryklund, L., and Sievertsson, H. (1978) Primary structure of somatomedin B: a growth hormone-dependent serum factor with protease inhibiting activity, *FEBS Lett. 87*, 55−60.
27. Ständker, L., Enger, A., Schulz-Knappe, P., Wohn, K. D., Germer, M., Raida, M., Forssmann, W. G., and Preissner, K. T. (1996) Structural and functional characterization of vitronectin-derived RGD-containing peptides from human hemofiltrate, *Eur. J. Biochem. 241*, 557−563.
28. Izumi, M., Shimo-Oka, T., Morishita, N., Ii, I., and Hayashi, M. (1988) Identification of the collagen-binding domain of vitronectin using monoclonal antibodies, *Cell Struct. Funct. 13*, 217−225.
29. Akama, T., Yamada, K. M., Seno, N., Matsumoto, I., Kono, I., Kashiwagi, H., Funaki, T., and Hayashi, M. (1986) Immunological characterization of human vitronectin and its binding to glycosaminoglycans, *J. Biochem. (Tokyo) 100*, 1343−1351.
30. Seiffert, D., and Loskutoff, D. J. (1991) Evidence that type 1 plasminogen activator inhibitor binds to the somatomedin B domain of vitronectin, *J. Biol. Chem. 266*, 2824−2830.
31. Seiffert, D., Ciambrone, G., Wagner, N. V., Binder, B. R., and Loskutoff, D. J. (1994) The somatomedin B domain of vitronectin. Structural requirements for the binding and stabilization of active type 1 plasminogen activator inhibitor, *J. Biol. Chem. 269*, 2659−2666.
32. Okumura, Y., Kamikubo, Y., Curriden, S. A., Wang, J., Kiwada, T., Futaki, S., Kitagawa, K., and Loskutoff, D. J. (2002) Kinetic analysis of the interaction between vitronectin and the urokinase receptor, *J. Biol. Chem. 277*, 9395−9404.
33. Philips, M., Johnsen, H., and Thorsen, S. (2000) Characterization of a complex between active plasminogen activator inhibitor-1 and N-terminal fragments of vitronectin from human placenta, *Fibrinolysis Proteolysis 14*, 22−34.
34. Kamikubo, Y., Okumura, Y., and Loskutoff, D. J. (2002) Identification of the disulfide bonds in the recombinant somatomedin B domain of human vitronectin, *J. Biol. Chem. 277*, 27109−27119.

35. Deng, G., Royle, G., Wang, S., Crain, K., and Loskutoff, D. J. (1996) Structural and functional analysis of the plasminogen activator inhibitor-1 binding motif in the somatomedin B domain of vitronectin, *J. Biol. Chem. 271*, 12716−12723.
36. Deng, G., Royle, G., Seiffert, D., and Loskutoff, D. J. (1995) The PAI-1/vitronectin interaction: two cats in a bag? *Thromb. Haemostasis 74*, 66−70.
37. Zhou, A., Huntington, J. A., Pannu, N. S., Carrell, R. W., and Read, R. J. (2003) How vitronectin binds PAI-1 to modulate fibrinolysis and cell migration, *Nat. Struct. Biol. 10*, 541−544.
38. Royle, G., Deng, G., Seiffert, D., and Loskutoff, D. J. (2001) A method for defining binding sites involved in protein−protein interactions: analysis of the binding of plasminogen activator inhibitor 1 to the somatomedin domain of vitronectin, *Anal. Biochem. 296*, 245−253.
39. Yatohgo, T., Izumi, M., Kashiwagi, H., and Hayashi, M. (1988) Novel purification of vitronectin from human plasma by heparin affinity chromatography, *Cell Struct. Funct. 13*, 281−292.
40. Kvassman, J. O., Lawrence, D. A., and Shore, J. D. (1995) The acid stabilization of plasminogen activator inhibitor-1 depends on protonation of a single group that affects loop insertion into beta-sheet A, *J. Biol. Chem. 270*, 27942−27947.
41. Schnölzer, M., Alewood, P., Jones, A., Alewood, D., and Kent, S. B. H. (1992) *In situ* neutralization in Boc-chemistry solid-phase peptide synthesis. Rapid, high yield assembly of difficult sequences, *Int. J. Pept. Protein Res. 40*, 180−193.
42. Jenne, D., and Stanley, K. K. (1985) Molecular cloning of S-protein, a link between complement, coagulation and cell-substrate adhesion, *EMBO J. 4*, 3153−3157.
43. Derua, R., Gustafson, K. R., and Pannell, L. K. (1996) Analysis of the disulfide linkage pattern in circulin A and B, HIV-inhibitory macrocyclic peptides, *Biochem. Biophys. Res. Commun. 228*, 632−638.
44. Delaglio, F., Grzesiek, S., Vuister, G. W., Guang, Z., Pfeifer, J., and Bax, A. (1995) NMRPipe: a multidimensional spectral processing system based on UNIX pipes, *J. Biomol. NMR 6*, 277−293.
45. Johnson, B. A., and Blevins, R. A. (1994) NMRView: A computer program for the visualization and analysis of NMR data, *J. Biomol. NMR 4*, 604−613.
46. Bax, A., Vuister, G. W., Grzesiek, S., Delaglio, F., Wang, A. C., Tschudin, R., and Zhu, G. (1994) Measurement of homo- and heteronuclear J-couplings from quantitative J correlation, *Methods Enzymol. 239*, 79−105.
47. Wishart, D. S., and Sykes, B. D. (1994) The ^{13}C chemical-shift index: A simple method for the identification of protein secondary structure using ^{13}C chemical-shift data, *J. Biomol. NMR 4*, 171−180.
48. Wishart, D. S., and Nip, A. M. (1998) Protein chemical shift analysis: a practical guide, *Biochem. Cell Biol. 76*, 153−163.
49. Wüthrich, K. (1986) *NMR of Proteins and Nucleic Acids*, John Wiley and Sons, New York.
50. Güntert, P., Mumenthaler, C., and Wüthrich, K. (1997) Torsion angle dynamics for NMR structure calculation with the new program DYANA, *J. Mol. Biol. 273*, 283−298.
51. Case, D. A., Pearlman, D. A., Caldwell, J. W., Cheatham, T. E., III, Wang, J., Ross, W. S., Simmerling, C. L., Darden, T. A., Merz, K. M., Stanton, R. V., Cheng, A. L., Vincent, J. J., Crowley, M., Tsui, V., Gohlke, H., Radmer, R. J., Duan, Y., Pitera, J., Massova, I., Seibel, G. L., Singh, U. C., Weiner, P. K., and Kollman, P. A. (2002) AMBER 7, University of California, San Francisco.
52. Cheatham, T. E., III, Cieplak, P., and Kollman, P. A. (1999) A modified version of the Cornell et al. force field with improved sugar pucker phases and helical repeat, *J. Biomol. Struct. Dyn. 16*, 845−862.
53. Constanciel, R., and Contreras, R. (1984) Self-consistent field-theory of solvent effect representation by continuum models − introduction of desolvation contribution, *Theor. Chim. Acta 65*, 1−11.
54. Tsui, V., and Case, D. A. (2000) Molecular simulations of nucleic acids using a generalized Born solvation model, *J. Am. Chem. Soc. 122*, 2489−2498.
55. Tsui, V., and Case, D. A. (2000) Theory and applications of the generalized born solvation model in macromolecular simulations, *Biopolymers 56*, 275−291.
56. Xia, B., Tsui, V., Case, D. A., Dyson, H. J., and Wright, P. E. (2002) Comparison of solution structures refined by molecular dynamics simulation in a vacuum, with a generalized Born model and with explicit water, *J. Biomol. NMR 22*, 317−331.
57. Laskowski, R. A., Rullmann, J. A. C., MacArthur, M. W., Kaptein, R., and Thornton, J. M. (1996) AQUA and PROCHECK-NMR: Programs for checking the quality of protein structures solved by NMR, *J. Biomol. NMR 8*, 477−486.
58. Hutchinson, E. G., and Thornton, J. M. (1996) PROMOTIF-A program to identify and analyze structural motifs in proteins, *Protein Sci. 5*, 212−220.
59. Koradi, R., Billeter, M., and Wüthrich, K. (1996) MOLMOL: A program for display and analysis of macromolecular structures, *J. Mol. Graphics 14*, 51−55.
60. Nicholls, A., Sharp, K. A., and Honig, B. (1991) Protein folding and association: insights from the interfacial and thermodynamic properties of hydrocarbons, *Proteins 11*, 281−296.
61. Liwo, A., Arlukowicz, P., Czaplewski, C., Oldziej, S., Pillardy, J., and Scheraga, H. A. (2002) A method for optimizing potential-energy functions by a hierarchical design of the potential-energy landscape: application to the UNRES force field, *Proc. Natl. Acad. Sci. U.S.A. 99*, 1937−1942.
62. Lee, J., Scheraga, H. A., and Rackovsky, S. (1997) New optimization method for conformational energy calculations on polypeptides: Conformational space annealing, *J. Comput. Chem. 18*, 1222−1232.
63. Späth, H. (1980) *Cluster Analysis Algorithms*, Halsted Press, New York.
64. Kazmierkiewicz, R., Liwo, A., and Scheraga, H. A. (2003) Addition of side chains to a known backbone with defined side-chain centroids, *Biophys. Chem. 100*, 261−280.
65. Jorgensen, W. L., Chandrasekhar, J., Madura, J., Impey, R. W., and Klein, M. L. (1983) Comparison of simple potential functions for simulating liquid water, *J. Chem. Phys. 79*, 926−935.
66. Braun, W., and Go, N. (1985) Calculation of protein conformations by proton−proton distance constraints. A new efficient algorithm, *J. Mol. Biol. 186*, 611−626.
67. Weiser, J., Shenkin, P. S., and Still, W. C. (1999) Approximate atomic surfaces from linear combinations of pairwise overlaps (LCPO), *J. Comput. Chem. 20*, 217−230.
68. Pascual, J., Martinez-Yamout, M., Dyson, H. J., and Wright, P. E. (2000) Structure of the PHD zinc finger from human Williams-Beuren syndrome transcription factor, *J. Mol. Biol. 304*, 723−729.
69. Duggan, B. M., Legge, G. B., Dyson, H. J., and Wright, P. E. (2001) SANE (Structure assisted NOE evaluation): an automated model-based approach for NOE assignment, *J. Biomol. NMR 19*, 321−329.
70. Shore, J. D., Day, D. E., Francis-Chmura, A. M., Verhamme, I., Kvassman, J., Lawrence, D. A., and Ginsburg, D. (1995) A fluorescent probe study of plasminogen activator inhibitor-1. Evidence for reactive center loop insertion and its role in the inhibitory mechanism, *J. Biol. Chem. 270*, 5395−5398.
71. Wind, T., Hansen, M., Jensen, J. K., and Andreasen, P. A. (2002) The molecular basis for anti-proteolytic and non-proteolytic functions of plasminogen activator inhibitor type-1: roles of the reactive centre loop, the shutter region, the flexible joint region and the small serpin fragment, *Biol. Chem. 383*, 21−36.
72. Sharp, A. M., Stein, P. E., Pannu, N. S., Carrell, R. W., Berkenpas, M. B., Ginsburg, D., Lawrence, D. A., and Read, R. J. (1999) The active conformation of plasminogen activator inhibitor 1, a target for drugs to control fibrinolysis and cell adhesion, *Structure 7*, 111−118.
73. Sui, G. C., and Wiman, B. (1998) Functional effects of single amino acid substitutions in the region of Phe113 to Asp138 in the plasminogen activator inhibitor 1 molecule, *Biochem. J. 331 (Pt 2)*, 409−415.
74. Jensen, J. K., Wind, T., and Andreasen, P. A. (2002) The vitronectin binding area of plasminogen activator inhibitor-1, mapped by mutagenesis and protection against an inactivating organochemical ligand, *FEBS Lett. 521*, 91−94.
75. Arroyo, D. P., Schroeck, F., Sinner, E. K., Muehlenweg, B., Twellmeyer, J., Sperl, S., Wilhelm, O. G., Schmitt, M., and Magdolen, V. (2002) Interaction of plasminogen activator inhibitor type-1 (PAI-1) with vitronectin, *Eur. J. Biochem. 269*, 184−192.

BI049647C